



Contents lists available at ScienceDirect

# Mechanical Systems and Signal Processing

journal homepage: [www.elsevier.com/locate/ymsp](http://www.elsevier.com/locate/ymsp)

## A PLL-based resampling technique for vibration analysis in variable-speed wind turbines with PMSG: A bearing fault case



Carlos M. Pezzani<sup>a,b,\*</sup>, José M. Bossio<sup>a,b</sup>, Ariel M. Castellino<sup>a</sup>,  
Guillermo R. Bossio<sup>a,b</sup>, Cristian H. De Angelo<sup>a,b</sup>

<sup>a</sup> Universidad Nacional de Río Cuarto, Fac. Ingeniería, Ruta Nacional #36, Km 601, Río Cuarto, Córdoba, Argentina

<sup>b</sup> Consejo Nacional de Investigaciones Científicas y Técnicas (CONICET), Ruta Nacional #36, Km 601, Río Cuarto, Córdoba, Argentina

### ARTICLE INFO

#### Article history:

Received 1 January 2016  
Received in revised form  
5 August 2016  
Accepted 11 August 2016

#### Keywords:

Bearing fault  
Vibrations analysis  
Resampling  
Order tracking  
Phased locked loop  
Wind turbine PMSG

### ABSTRACT

Condition monitoring in permanent magnet synchronous machines has gained interest due to the increasing use in applications such as electric traction and power generation. Particularly in wind power generation, non-invasive condition monitoring techniques are of great importance. Usually, in such applications the access to the generator is complex and costly, while unexpected breakdowns results in high repair costs. This paper presents a technique which allows using vibration analysis for bearing fault detection in permanent magnet synchronous generators used in wind turbines. Given that in wind power applications the generator rotational speed may vary during normal operation, it is necessary to use special sampling techniques to apply spectral analysis of mechanical vibrations. In this work, a resampling technique based on order tracking without measuring the rotor position is proposed. To synchronize sampling with rotor position, an estimation of the rotor position obtained from the angle of the voltage vector is proposed. This angle is obtained from a phase-locked loop synchronized with the generator voltages. The proposed strategy is validated by laboratory experimental results obtained from a permanent magnet synchronous generator. Results with single point defects in the outer race of a bearing under variable speed and load conditions are presented.

© 2016 Elsevier Ltd. All rights reserved.

## 1. Introduction

In general, wind turbines (WT) are placed away from crowded areas or at inaccessible places while they are exposed to severe operation environments. In this context, application of condition-based maintenance and fault diagnosis, becomes significantly important [1,2]. The proper planning of maintenance operations as well as the early detection of faults reduces operation and maintenance (O&M) costs while also increases the system reliability [2].

Since WT are complex electromechanical systems, several components can fail or operate under abnormal conditions. Among these possible faults, those associated to the turbine, the coupling between the turbine and the generator, the generator itself, as well as to the power electronic converters and the electrical system can be mentioned [2]. In particular, the use of permanent magnet synchronous generators (PMSG) in WT has become one of the most important applications these days. This is mainly due to the fact that PMSG are characterized by high power density and high performance. It allows

\* Corresponding author at: Universidad Nacional de Río Cuarto, Fac. Ingeniería, Ruta Nacional #36, Km 601, Río Cuarto, Córdoba, Argentina.  
E-mail address: [cpezzani@ing.unrc.edu.ar](mailto:cpezzani@ing.unrc.edu.ar) (C.M. Pezzani).

building generators with high number of poles in direct driven WT, thus avoiding the use of heavy gearboxes.

Several diagnostic efforts have been focused on generator, gearbox, and bearings [1–3]. However, bearing problems represents the fault with highest rate of occurrence among electrical machines and rotating equipment in general [4–6]. For WT applications it becomes very attractive the early detection of this faults to optimize the O&M costs. Recently, different strategies based on the analysis of electrical variables to detect bearing faults have been developed [7,8]. These strategies have notable features in common: they do not require the assembly of additional sensors, while can be implemented avoiding direct access to the machine. However, the low signal-to-noise ratio and the complex techniques used to process signals make their application difficult.

Recently, some proposals that uses measurement of temperature [9] or acoustic emission [10] to detect bearing problems have also been presented. Nevertheless, the analysis of mechanical vibrations represent the most commonly used and accepted technique for bearing fault detection in rotating machines. In addition, WTs have vibration sensors at strategic points to monitor the condition of their different components. Thus, the analysis of vibrations becomes very important for the detection of bearing faults in such applications [11–14].

The problems that arise when analyzing vibrations in wind generation applications are mainly due to the fact that WTs normally operate at variable speed, depending thus on wind conditions. Such rotational-speed variability feature complicates the use of traditional vibration analysis based on Fourier Transform (FT).

To solve these problems, the use of tools such as wavelets [11] or statistical analysis [13] have been proposed. Another choice to address the fault detection problem under time-varying conditions is the use of strategies based on Order Tracking (OT) [16]. This technique consists in sampling the vibration signals so as to synchronize them fully with the rotor angular position and then analyze the signal frequency spectrum. Different strategies based on OT have been proposed for the detection of bearing faults in WTs [17–20]. Traditional OT techniques use signals from an encoder or tachometer to obtain the rotor angular position [17,18]. However, to avoid using an extra sensor, different techniques based on estimation have been proposed. A strategy for the detection of faults based on OT that obtains information about speed directly from the envelope of vibration signals is presented in [19]. In [20], a strategy for vibration resampling is presented for the detection of mechanical unbalances in wind generators with PMSG. Rotor angular position is obtained from voltage measurements using a reduced-order observer, which shows robustness under voltage disturbances.

A strategy for the detection of bearing faults in WT with PMSG based on resampling of mechanical vibration signals, is proposed in this work. The proposal allows using the known vibration spectrum analysis to identify the components associated to bearing faults, even under variable speed operation. With this aim, vibration signals are resampled synchronized with the estimated rotor position, which is obtained from the measurement of the generator voltages and using of a Phase-locked loop (PLL). PLL are commonly used to synchronize generation and harmonic compensation systems by means of active power filters [21–23] and show to work properly for disturbed voltage conditions. Thus, the proposed strategy neither requires a rotor position sensor nor the generator parameters.

The paper is organized as follows: a brief description of common bearing faults and their characteristic frequencies are presented in Section 2. The proposed strategy and the PLL used for the estimation of rotor angular position are presented in Section 3. Finally, Section 4 shows the experimental results obtained from a PMSG with faulty bearing to validate the proposed strategy.

## 2. Bearing faults

Depending on the relative size of the affected area, bearing faults can be classified into two main groups, generalized faults and localized or single-point faults. Generalized faults are characterized by a damaged area covering an important portion of the affected components, either races or rolling elements. In general, faults of this type are due to normal wear and tear and occasionally due to current circulation through the bearing, commonly observed in motors fed by variable speed drives. On the other hand, single-point defects affect small areas of the bearing components and are mainly due to high concentration of internal forces [12,15].

The analysis of mechanical vibrations is the most common strategy for detecting bearing faults. In the frequency spectrum of vibrations, single-point defects become evident by means of components with a characteristic and well-defined frequency for each bearing component. Such frequencies depend on the geometry of the bearing and on the relative velocity between the fault and the rolling elements. Thus, the fault frequency for each bearing element may be determined as follows [15]:

Outer-race fault frequency,

$$f_o = \frac{n}{2} f_r \left[ 1 - \frac{D_b \cos(\beta)}{D_c} \right] \quad (1)$$

Inner-race fault frequency,

$$f_i = \frac{n}{2} f_r \left[ 1 + \frac{D_b \cos(\beta)}{D_c} \right] \quad (2)$$

Cage fault frequency,

$$f_c = \frac{1}{2}f_r \left[ 1 - \frac{D_b \cos(\beta)}{D_c} \right] \tag{3}$$

Ball fault frequency,

$$f_b = \frac{D_c}{2D_b} f_r \left[ 1 - \frac{D_b^2 \cos^2(\beta)}{D_c^2} \right] \tag{4}$$

here  $n$  is the number of balls (or rolling elements),  $D_b$  is the ball diameter,  $D_c$  is the mean diameter of the cage,  $\beta$  is the contact angle and  $f_r$  is the rotational frequency.

### 3. Proposed strategy

For single-point bearing faults, the spectral analysis of mechanical vibrations is commonly used as detection technique. Since WTs normally operate at variable speed, a resampling technique based on OT is proposed to minimize the leakage effects on the vibration spectrum. Unlike conventional OT strategies that require measurement of rotor angular position, the proposed strategy uses an estimation of the rotor based on the measurement of generator voltages and a PLL. In steady state operation, or under slow-speed variations, the angular position of the voltage space vector of the PMSG is directly related to the rotor angular position. Thus, under these conditions, it is possible to employ the voltage vector angle as an acceptable estimation of the angular position. This estimated angular position is used to resample the vibration signals at constant increments of angular position and then calculate the Fast Fourier Transform to identify the characteristic fault components in the obtained vibration spectrum. Fig. 1 shows a scheme of the proposed strategy. For its implementation, it requires at least one vibration acceleration signal and two stator line voltages from the PMSG. The following sections briefly describe the implemented resampling strategy and the PLL used to estimate the angular position.

#### 3.1. Sampling at constant increments of angular position

The vibration pattern of a rotating machine depends on the position of rotating parts, and therefore on rotation speed. At constant rotation speed, acquiring vibration signals at constant sampling frequency is equivalent to sampling at constant increments of the angular rotor position. However, if speed varies during the sampling period, then the previous statement is no longer valid. In such case, it will be difficult to identify the specific fault components in the obtained vibration spectrum due to its high dispersion. To overcome this problem, the common procedure is to acquire the vibration signals synchronously with rotor position. Sampling vibration signals synchronized with rotor position usually requires additional hardware, specially designed for this task. In high power WT, the cost of this additional hardware can be justified, but this does not occur in medium/low power turbines. In these cases, re-sampling based strategies (or order tracking – OT techniques) are more suitable.

Traditional approaches based on OT acquire the signals at constant sampling frequency ( $\Delta t = \text{const.}$ ) and then, from the measured rotor position, the signals are resampled at constant angle increments ( $\Delta\theta = \text{const.}$ ).

Consider the vector of vibration signal data  $\vec{x} = [x_{(1)} \ x_{(2)} \ x_{(3)} \ \dots \ x_{(n)}]$ , measured at constant sample intervals, and the vector of rotor angular position data  $\vec{\theta}_r = [\theta_{r(1)} \ \theta_{r(2)} \ \theta_{r(3)} \ \dots \ \theta_{r(n)}]$ , obtained at the same sampling instants.

Then, the vector of angular positions is redefined at equally-spaced angular positions,

$$\vec{\theta}'_r = [\theta'_{r(1)} \ \theta'_{r(2)} \ \theta'_{r(3)} \ \dots \ \theta'_{r(n)}] = [\theta_{r(1)} \ \theta_{r(1)} + \Delta\theta \ \theta_{r(1)} + 2\Delta\theta \ \dots \ \theta_{r(n)}],$$

with

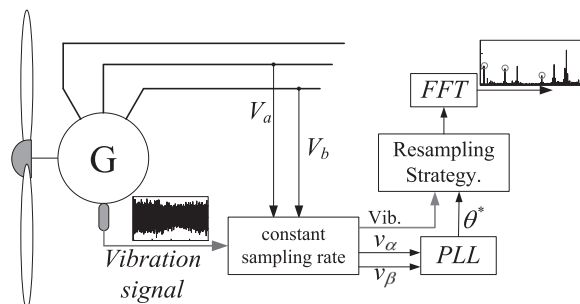


Fig. 1. Scheme of the proposed resampling strategy for vibration analysis in PMSG.

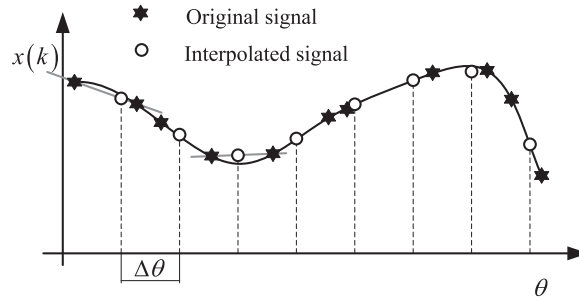


Fig. 2. Resampling at constant angle increments.

$$\Delta\theta = \theta'_{r(k+1)} - \theta'_{r(k)} = \frac{\theta_{r(n)} - \theta_{r(1)}}{n - 1}$$

These angular positions are used to resample the vibration signal data by interpolation, as shown in Fig. 2, thus obtaining the new vibrations signal resampled at constant angular intervals,  $\vec{x}' = [x'_{(1)} \ x'_{(2)} \ x'_{(3)} \ \dots \ x'_{(n)}]$ .

The main problem for implementing these techniques is the need for a vector of rotor position data with the required resolution. Depending of the particular application, an optical encoder or other position sensor used for controlling the PMSG may be available. However, when a position sensor is not available, a sensor-less technique must be implemented.

The following subsection shows the implementation of the resampling technique using the generator voltages without having to measure the angular rotor position.

### 3.2. Estimation of the angular position of the voltage vector

Considering the complex variable PMSG model with sinusoidal EMF in a stationary reference frame,

$$\begin{aligned} v_{\alpha\beta} &= (r_s + L_s p)i_{\alpha\beta} + \varepsilon_{\alpha\beta} \\ \varepsilon_{\alpha\beta} &= \lambda_m \omega_r e^{-j\theta_r} \end{aligned} \tag{5}$$

where  $r_s$  is the stator resistance,  $L_s$  the stator leakage inductance,  $\varepsilon_{\alpha\beta}$  the induced stator EMF and  $\lambda_m$  the peak flux linkage of the permanent magnets.

From (5), it is clear that if the generator is no-loaded, the output voltage is directly the induced EMF ( $\varepsilon_{\alpha\beta}$ ). In such conditions, rotor angular position can be determined from the measured output voltages as follows,

$$\theta_r \approx \arctan\left(\frac{\varepsilon_\beta}{\varepsilon_\alpha}\right) \tag{6}$$

On the other hand, if the generator is loaded, stator current will not be null and the output voltage will be different from the induced EMF due to the voltage drop in the generator leakage impedance. While the machine operates at steady state, the phase difference between the EMF and the output voltage will be constant and small. Then, the measured voltages can still be used to obtain a vector of equally-spaced angular rotor positions. However, if the load is non-linear, current harmonics introduces distortions in the output voltages, which produce errors in the rotor position calculus using (6). To overcome this problem, in this work it is proposed to estimate the angle of the output voltage vector using a positive-sequence detector based on a Phase-Locked Loop. In particular, a *Dual Second Order Generalized Integrator PLL*, (DSOGI-PLL) [22] was implemented to determine the angular position of the voltage vector. This configuration seems to be more robust to voltage distortions and disturbances, and its implementation is quite simple [23]. Fig. 3 shows a scheme of the implemented PLL.

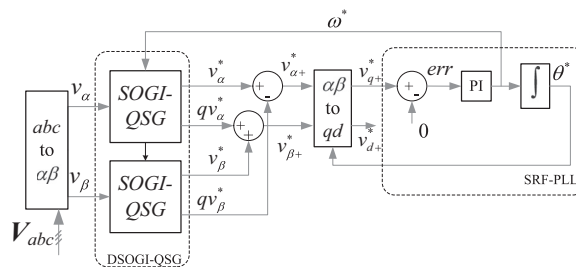


Fig. 3. Implemented phase locked loop (DSOGI-PLL).

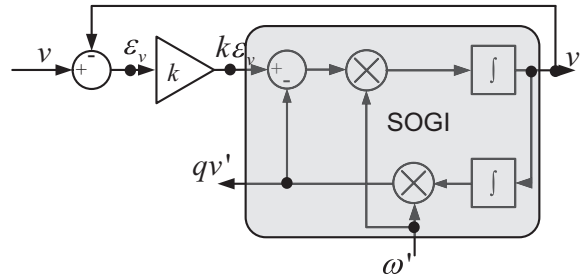


Fig. 4. Second Order Generalized Integrator – Quadrature Signal Generators (SOGI-QSG).

From the measured line to line stator voltages, the  $\alpha\beta$  components are obtained using the following transformation,

$$\begin{bmatrix} v_\alpha \\ v_\beta \end{bmatrix} = \frac{2}{3} \begin{bmatrix} 1 & \frac{1}{2} \\ 0 & \frac{\sqrt{3}}{2} \end{bmatrix} \begin{bmatrix} v_{ab} \\ v_{bc} \end{bmatrix} \tag{7}$$

In order to avoid the disturbance in the calculation of the angular position introduced by load unbalance or distortions, this angle must be calculated from the positive-sequence components of the measured voltages, which can be calculated as follows,

$$\begin{bmatrix} v_{\alpha+} \\ v_{\beta+} \end{bmatrix} = \frac{1}{2} \begin{bmatrix} 1 & -q \\ q & 1 \end{bmatrix} \begin{bmatrix} v_\alpha \\ v_\beta \end{bmatrix} \tag{8}$$

where  $q$  is a  $\pi/2$  phase-shift operator, which means the in-quadrature signal of the original waveform.

Such quadrature signals are obtained using two Second Order Generalized Integrator – Quadrature Signal Generators (SOGI-QSG), shown in Fig. 4, one for each voltage component.

The transfer functions of the SOGI-QSG are the following,

$$\begin{aligned} \frac{v^*}{v}(s) &= \frac{k\omega^*s}{s^2 + k\omega^*s + \omega^{*2}} \\ \frac{qv^*}{v}(s) &= \frac{k\omega^{*2}}{s^2 + k\omega^*s + \omega^{*2}} \end{aligned} \tag{9}$$

where  $\omega^*$  is the resonance frequency and  $k$  is the damping factor. The amplitude of the obtained in-quadrature signals ( $v^*$  and  $qv^*$ ) will be equal to the amplitude of the input signal  $v$  when the frequency of the input signal matches the resonance frequency ( $\omega^*$ ) [24].

For this reason, a frequency adaptation loop must be implemented in order to obtain the correct in-quadrature signals necessary for the positive-sequence voltages calculation. With this aim, the obtained  $\alpha\beta$  positive-sequence voltages are projected to a synchronous reference frame,

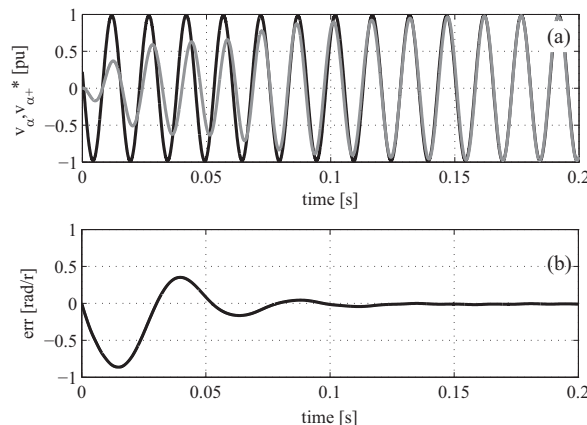


Fig. 5. Performance of the implemented PLL. a) PMSG Voltage  $v_\alpha$  (black line) and estimated positive sequence component voltage  $v_{\alpha+}^*$  (gray line). b) Estimation error.

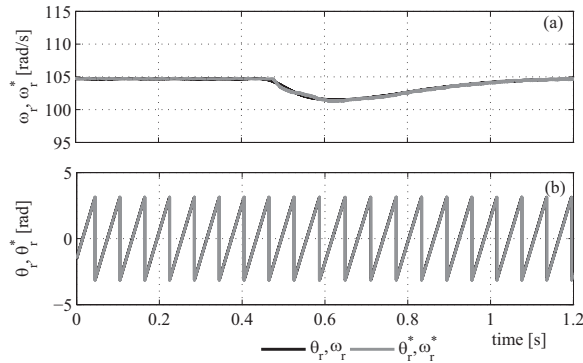


Fig. 6. Performance of the implemented PLL. (a)  $\omega_r$  and  $\omega_r^*$ . (b)  $\theta_r$  and  $\theta_r^*$ . Actual waveforms (black line) and waveforms obtained from the PLL (gray line).

$$\begin{bmatrix} v_{d+}^* \\ v_{q+}^* \end{bmatrix} = \begin{bmatrix} \cos(\theta^*) & \sin(\theta^*) \\ -\sin(\theta^*) & \cos(\theta^*) \end{bmatrix} \begin{bmatrix} v_{\alpha+}^* \\ v_{\beta+}^* \end{bmatrix} \tag{10}$$

In this reference frame, a Synchronous Reference Frame Phase-Locked Loop (SRF-PLL) is implemented in order to track the generator frequency and then adapt the DSOGI-QSG resonance frequency, as proposed in [22]. The SRF-PLL is composed by a Proportional+Integral (PI) regulator that brings the  $v_{q+}^*$  component to zero by adjusting the reference-frame angular position. This allows estimating both, the angular frequency and the angular position of the positive-sequence voltage vector.

As it was demonstrated in [22,24], the DSOGI-PLL acts as a low-pass filter for the positive-sequence component, and as a notch filter for the negative-sequence component. Besides, it provides a good attenuation of high-order harmonics. This makes it very suitable for positive-sequence detection, being robust to voltage unbalances and disturbances. Tuning of the DSOGI-PLL can be obtained by setting  $k$  and the PI gains. This results in a trade-off between the bandwidth of the SOGI and its sensitivity to voltage harmonics and noise [24].

Figs. 5 and 6 present a brief analysis of the performance of the implemented PLL. Both the DSOGI block gains and the PI constants were determined so as to achieve an acceptable performance for the characteristic voltage waveforms of the available PMSG.

Fig. 5 shows a detail of the PLL synchronization with the generator operating at constant speed  $\sim 460$  r/s. Fig. 5(a) shows the estimated voltage  $v_{\alpha+}^*$  (gray line) and the actual generator voltage  $v_{\alpha}$  (black line). In Fig. 5(b) the evolution of the estimation error is shown. As can be appreciated, the PLL reaches the synchronism in a few cycles.

Fig. 6 shows the behavior under a disturbance in the generator speed. The actual PMSG speed is shown in black line in Fig. 6(a), while the estimated speed is shown in gray line. Fig. 6(b) shows the actual (black) and estimated (gray) rotor positions. As can be seen, no significant differences can be found between the estimated and actual signals. In these tests, a resolver was used to measure the generator speed and angular position.

As the expected variations on the generator rotational speed are slow compared to the electrical dynamics, the dynamic performance of the implemented PLL is fast enough to use the estimation of the voltage vector angular position,  $\theta^*$ , as a good approximation of the rotor angular position of the PMSG. Then, this information can be used for vibration signal resampling. The performance of the proposed resampling technique using the estimated position is presented in the next section.

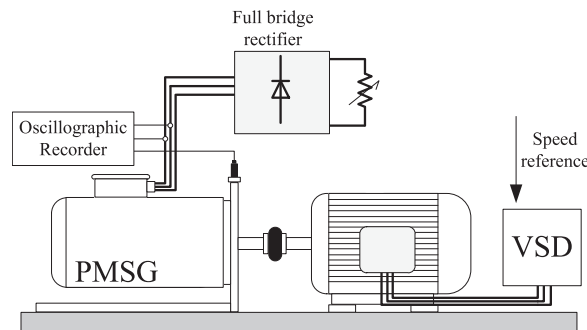


Fig. 7. Experimental test bench.

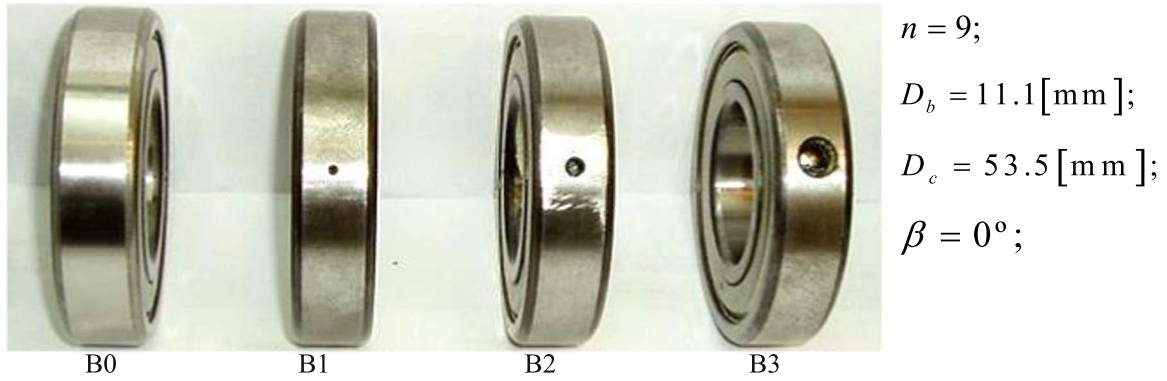


Fig. 8. Healthy bearing and bearings with a single-point defect on outer race.

#### 4. Experimental results

To validate the proposed strategy, measurements were made on an experimental prototype that consists of a PMSG with the possibility of include a bearing fault. Several cases were analyzed corresponding to the PMSG with and without bearing faults and at constant and variable speed. During testing, two line voltages of the generator and a vibration acceleration signal corresponding to the vertical axis were measured. These signals, sampled at constant frequency, were processed on a personal computer where the proposed resampling strategy was implemented. A brief description of the technical characteristics of the experimental prototype and the results obtained with the proposed strategy are included in the following subsections.

##### 4.1. Experimental prototype

Fig. 7 shows a scheme of the test bench used for experimental tests. The test bench consists of the PMSG under analysis directly coupled to a 5.5 kW induction motor. The induction motor is powered by a variable-speed drive (VSD), which allows modifying and controlling the generator rotational speed. The tested generator corresponds to a PMSG of 3.5 kW and 380 V whose main parameters are listed in Table A.1 in Appendix A. For vibration measurements, a piezoelectric accelerometer placed on the faulty bearing side of the generator was used. In addition, to measure the generator voltages, isolated voltage probes (200 MHz bandwidth, 10:1) were used. All the signals are acquired using an oscillographic recorder at 10 kS/s.

To include bearing faults in the PMSG, the original bearing corresponding to the coupling side was replaced by an identical one but with a single point defect on the outer race. This fault was artificially created by drilling a hole on the outer race through electro-erosion. Fig. 8 shows the healthy bearing and the bearings with a single-point defect in outer race (6, 4 and 2 mm-diameter holes). This figure also shows a detail of the dimensions and characteristics of the bearings. A three-phase full-bridge rectifier connected to a resistive load composes the generator load. Because the generator has a high impedance, the resulting voltages when the load is connected are not purely sinusoidal. This validates the strategy under distorted voltage conditions, which is similar to practical applications of wind generation where the generator is connected to a back-to-back converter.

##### 4.2. Results

For bearings shown in Fig. 8, the fault characteristics frequencies for each element (Eqs. (1)–(4)) are shown in Table 1. As the PMSG can operate at different speed, the frequencies shown in Table 1 are expressed in per unit (pu) of rotating frequency. Then, for a single point defect in outer race, frequency components at  $f_0 k = 3.6k$  (with  $k = 1, 2, \dots$ ) are introduced in the vibration spectrum.

Table 1  
Characteristic fault frequencies (pu).

$k$	Element			
	$f_o$	$f_i$	$f_c$	$f_b$
1	3.6	5.4	0.4	1.9
2	7.1	10.9	0.79	3.8
⋮	⋮	⋮	⋮	⋮

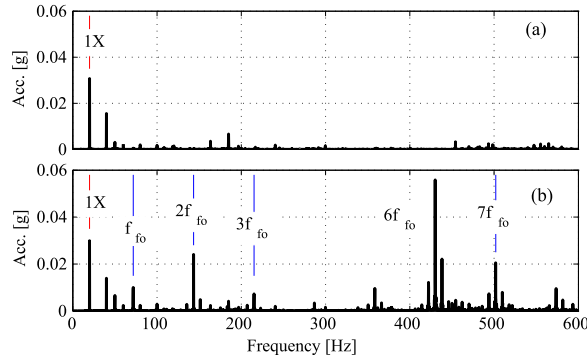


Fig. 9. Vibration acceleration spectrum at constant speed: (a) without bearing fault and, (b) with bearing fault (Bearing B3 6 mm).

#### 4.2.1. Vibration analysis at constant speed

The first tests were performed with the generator operating at constant speed, in order to obtain the reference spectra for faulty and healthy cases, and verify the appearance of components given by Table 1. From these tests, acceleration frequency spectra were obtained using FFT without resampling. Fig. 9 shows two frequency spectra of vibration acceleration for the PMSG operating at constant speed. Fig. 9(a) corresponds to the PMSG without bearing fault, and (b) with a single-point defect on the outer race (B3 6 mm). The test was carried out at a 1200 rpm rotation speed, then, the rotational frequency component (1X) can be observed at 20 Hz. It can also be concluded from Fig. 9(a) that the most significant components in the frequency spectrum correspond to the rotational frequency (1X) and its multiples. On the other hand, for the case with outer race single-point defect the spectral components due to bearing fault can be clearly observed (Fig. 9(b)).

#### 4.2.2. Vibration analysis at variable speed

The cases presented in the previous section shows that if the rotation speed of the generator is constant, then the traditional vibration analysis can be used. However, when the rotation speed undergoes variations during the recording of signals, difficulties arise. Fig. 10 shows the vibration analysis for a case with bearing fault and the PMSG with variations in the rotation speed during the sampling period. During this particular test, the mean rotation speed was 1100 rpm ( $\sim 115$  r/s). Fig. 10(a) shows the rotational speed of PMSG and Fig. 10(b) the frequency spectrum of the vibration signal. As it can be observed in this figure, speed variations produce a significant dispersion in the vibration spectrum. This effect makes impossible to identify the components related to the fault.

Fig. 11 shows the spectrum of the voltage and vibration signals for the same case, after applying the proposed resampling strategy. From the figure, it can be clearly observed in the frequency spectrum the components due to rotation and to fault. In order to clearly identify the components of interest in the spectrum, the frequency axis was normalized with generator rotation frequency (1X). Fig. 11(a) shows that only one component corresponding to the fundamental electrical frequency appears in the spectrum of the generator voltage. Since the tested PMSG has 8 poles, the electrical fundamental frequency is located at 4X.

By analyzing the frequency spectrum of the vibration acceleration (Fig. 11(b)), it can be observed the components due to bearing fault. The fault frequency in the outer race,  $f_0$ , and some of its multiples are highlighted in the spectrum. By comparing the vibration spectra shown in Fig. 10(b) (without resampling) and Fig. 11(b) (resampling), it can be concluded that the proposed strategy allows making a correct diagnosis even when speed is not constant.

Comparing Fig. 11(b) with Fig. 9(b) (constant speed), it is observed that the amplitude of the components is lower in the variable speed case. This is due to the mean speed of the variable speed test is lower than in the constant speed case. Then,

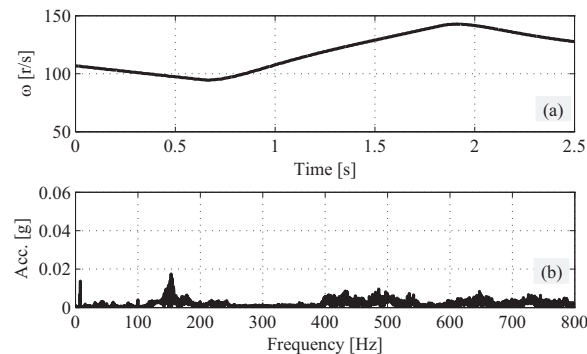
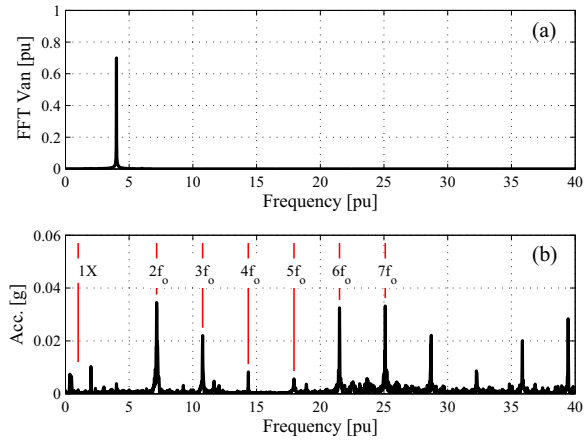


Fig. 10. (a) PMSG rotational speed; (b) spectrum of vibration acceleration without resampling. Bearing fault case (Bearing B3 6 mm).



**Fig. 11.** (a) Spectrum of PMSG voltage, and (b) spectrum of vibration acceleration with the proposed resampling strategy. Bearing fault case (Bearing B3 6 mm).

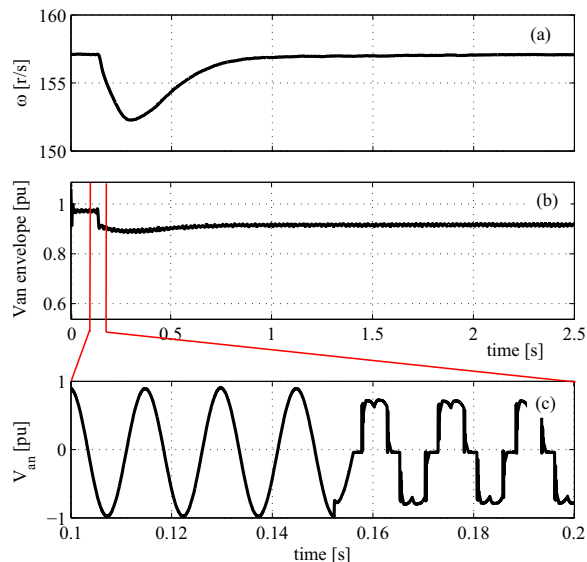
the global vibration value is lower in a similar way. This effect could be compensated by scaling vibration measurements according to the generator speed.

#### 4.2.3. Vibration analysis at variable speed, loaded generator case

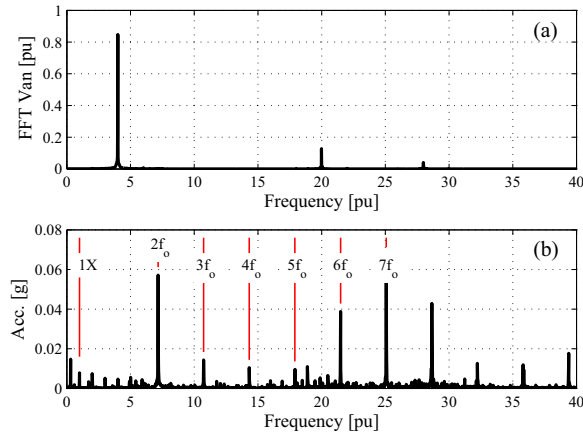
In order to show the robustness of the proposed strategy to changes and disturbances on the generator load, Figs. 12 and 13 present the case when a 1 kW load is suddenly connected to the generator at  $t=300$  ms. Initially, the PMSG was working unloaded, at rated speed. Fig. 12 shows the envelope of generator phase voltage, the rotational speed during the described test and the waveform of the generator voltage at the instant when the load is connected. As it can be seen, when load is connected the machine speed suffers a disturbance, which is compensated by the speed controller of the driving machine (Fig. 12(a)). The dynamics of the speed transient depends on the speed controller parameters and the inertia of the driving-generator set. A decrease in the generator voltage is appreciated in Fig. 12(b), due to the voltage drop in the generator stator impedance. Moreover, when the load is connected, due to generator inductance and the three-phase rectifier load, the generator voltage results highly distorted, as can be seen in Fig. 12(c). This allows validating the strategy under distorted voltage conditions.

Fig. 13(a) shows the frequency spectrum of the generator voltage, while Fig. 13(b) presents the spectrum of the vibration acceleration, both after applying the proposed resampling strategy. In this case, in the voltage spectrum the fundamental electrical frequency component and the harmonics introduced by the rectifier can be identified.

Furthermore, on the acceleration vibration spectrum, the components due to the outer-race single-point bearing defect can be clearly appreciated. Comparing the spectrum of Fig. 13(b) with the one shown in Fig. 11(b), it can be seen that the



**Fig. 12.** (a) PMSG rotational speed; (b) PMSG voltage envelope; (c) detail of the PMSG voltage waveform. Sudden load change case, with bearing fault.



**Fig. 13.** (a) Spectrum of PMSG voltage, (b) spectrum of vibration acceleration with the proposed resampling strategy. Sudden load change case, with bearing fault (Bearing B3 6 mm).

amplitude of the components are slightly different, due to the difference in the mean speed. This change in the rotor speed produce that different vibration modes are excited, thus some frequency components are increased while other components are reduced.

4.2.4. Sensitivity analysis

The previously presented results correspond to experimental cases obtained with a bearing with a 6 mm single-point defect in the outer race (Bearing B3 in Fig. 8). In order to analyze the sensitivity of the proposal in front of different fault severities, additional tests were performed using bearing with less severe faults (Bearings B1 and B2 with 2 and 4 mm single-point defects in the outer race, respectively, shown in Fig. 8). Different operational conditions were tested for the three bearings: Case 1: constant rotational speed (1500 rpm); Case 2: ± 20% speed oscillation around 1000 rpm; Case 3: speed increase from 500 rpm to 1000 rpm; Case 4: sudden connection of the generator load at 1000 rpm. In all the cases, two line voltages and vertical acceleration vibration were measured, and the proposed re-sampling technique was applied.

A severity factor is proposed to weight the considered faults and compare the results for different bearing faults. This severity factor is given by the sum of the first 8 fault frequency components of the acceleration vibration spectrum, i.e.

$$SF_{f_0} = \sum_{k=1}^8 a_{f_0}(k) \tag{11}$$

where  $a_{f_0}(k)$  represents the amplitude of the component at the frequency  $f_0 k$ , ( $k = 1, 2, \dots$ ). The number of components considered in  $SF_{f_0}$  was selected in order to obtain a clear separation between the considered fault cases.

The fault severity factor ( $SF_{f_0}$ ), obtained for the three bearings and the operating conditions described as 1–4, are presented in Table 2. In all the cases, the values are expressed in g.

From all the performed tests, the obtained results show that the proposed technique does not significantly affect the amplitude of the vibration spectrum components, thus allowing to distinguish between the different fault severity cases even under different operating conditions. Is worth mentioning that the proposed fault severity factor only allows to compare the results and to distinguish between the different faults cases, but does not enable to absolutely quantify the bearing fault severity. On the other hand, since the proposed technique does not perform any additional processing of the vibration signal, the ability to correctly identify the fault components is directly associated with the signal-noise ratio of the original vibration signal.

The proposed re-sampling technique can be compared with other proposals available in the literature. Different reference signals are used to perform the vibration signal resampling, and then become independent of the speed variations.

**Table 2**  
Fault severity factor ( $SF_{f_0}$ ).

Case	Bearing		
	B1 (Fault 2 mm)	B2 (Fault 4 mm)	B3 (Fault 6 mm)
Case 1	0.062	0.92	1.5
Case 2	0.093	0.61	1.6
Case 3	0.085	0.76	2.0
Case 4	0.072	0.59	1.6

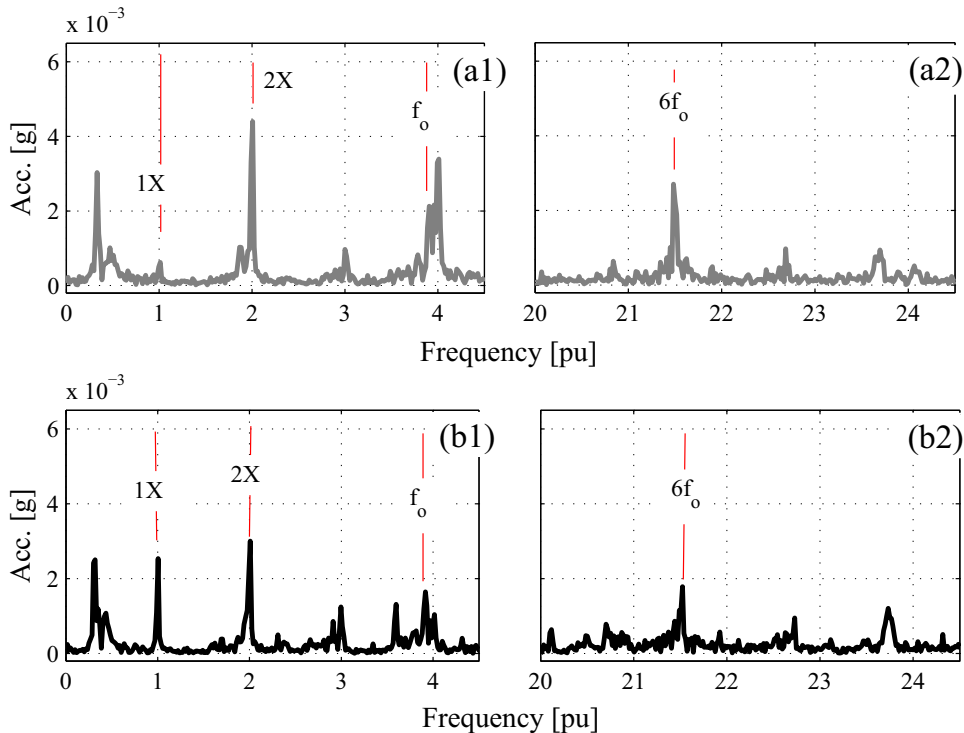


**Fig. 14.** Spectrum of vibration acceleration with bearing fault (Bearing B1 2 mm). (a) Resampling with actual angular rotor position, (b) proposed resampling strategy.

From all of them, those which uses the rotor position measurement obtained from a digital encoder can be considered as the one which offers the greater resolution.

With the aim of qualitatively evaluate the effect of the proposal regarding spectrum resolution and dispersion introduced by the use of the PLL based position information, it was compared with the same technique but using the actual angular rotor position signal for resampling.

Different tests were performed with the B1 bearing (2 mm single point defect), were besides the measurement of the generator voltages and vertical vibration acceleration, the rotor position was measured using a resolver. The smaller fault case was selected due to it is the most unfavorable case regarding spectrum resolution and signal-noise ratio in order to identify the fault components.

Fig. 14 shows the results for a variable speed test, where the vibration spectra obtained with the proposed resampling technique are presented in part (b), while the spectra obtained from the resampling using the actual measured position are presented in part (a).

Parts (a1) and (b1) show a detail of the spectrum around 1 and 5 pu components, while parts (a2) and (b2) correspond to the spectrum around components 20–25 pu. In these figures, the first two multiples of the rotation speed, and the fault components  $f_o$  and  $6f_o$  can be clearly identified. As can be appreciated, the proposed rotor angle estimation does not introduce any significant distortion in the resultant vibration spectrum.

## 5. Conclusions

A strategy for resampling vibration signals used for bearing faults analysis in PMSG is presented in this paper. The proposed strategy is designed to be used in variable-speed wind power applications. As in such applications the rotation speed varies depending on the wind conditions, a resampling technique is proposed to obtain vibration signals synchronized with the rotor position. Particularly, the proposed technique is a tracking-order technique that consists in sampling vibration signals at constant intervals of the rotor angular position. This allows obtaining a vibration frequency spectrum without dispersion due to variations in the rotation speed. Traditional tracking-order techniques use measurements to obtain the rotor position which implies having an additional sensor. Unlike them, the estimation of the rotor position from the generator voltages is proposed in this paper. A phase-locked loop DSOGI- PLL which is robust to load and voltage disturbances, was used for position estimation. The proposed scheme does not require the rotor position or the generator parameters. Experimental results obtained from a PMSG with a bearing fault validate the proposed strategy. Tests are carried out at both constant speed and variable speed, including a sudden load connection and different fault severities.

Besides, the performance of the phase-locked loop is analyzed in detail. Results show that the resampling technique allows reliably identifying the components due to localized faults in the vibration spectrum even at variable speed and with voltage distortion.

Even when the proposed strategy was implemented off-line, from measured vibration and voltage signals, it could also be implemented for on-line condition monitoring with slight modifications. Since the strategy was validated only in the laboratory with a passive load connected to the generator, in future studies a test bench will be implemented with a back-to-back converter interconnecting the generator with the power grid. This configuration will allow evaluating the effects of higher voltage distortions introduced by the converter over the proposed strategy, and also the effects of the generator controller on its dynamic performance.

## Acknowledgments

This work is supported in part by the Consejo Nacional de Investigaciones Científicas y Técnicas (CONICET) of Argentina, and the Facultad de Ingeniería, Universidad Nacional de Río Cuarto (UNRC).

## Appendix A

See Table A1.

**Table A.1**

PMSG technical data and parameters.

Nominal torque	16.6	Nm
Nominal current	7.7	A
Nominal power	3.5	kW
Nominal speed	2000	rpm
Inertia	0.0046	kg m <sup>2</sup>
Poles	8	–
$r_s$	1.396	–
$L_s$	9.354	mH
$\lambda_m$	0.297	Wb/m <sup>2</sup>

## References

- [1] F.P. García Márquez, A.M. Tobias, J.M. Pinar Pérez, M. Papaalias, Condition monitoring of wind turbines: techniques and methods, *Renew. Energy* 46 (2012) 169–178.
- [2] W.Y. Liu, B.P. Tang, J.G. Han, X.N. Lu, N.N. Hu, Z.Z. He, The structure healthy condition monitoring and fault diagnosis methods in wind turbines: a review, *Renew. Sustain. Energy Rev.* 44 (2015) 466–472.
- [3] I. Antoniadou, G. Manson, W.J. Staszewski, T. Barszcz, K. Worden, A time–frequency analysis approach for condition monitoring of a wind turbine gearbox under varying load conditions, *Mech. Syst. Signal Process.* 64–65 (2015) 188–216.
- [4] I. El-Thalji, E. Jantunen, A summary of fault modelling and predictive health monitoring of rolling element bearings, *Mech. Syst. Signal Process.* 60–61 (2015) 252–272.
- [5] Report of Large Motor Reliability Survey of Industrial and Commercial Installations, Part I, *IEEE Transactions on Industry Applications*, IA-21, 1985, pp. 853–864.
- [6] P.J. Tavner, Review of condition monitoring of rotating electrical machines, *Electr. Power Appl., IET* 2 (2008) 215–247.
- [7] A. Picot, Z. Obeid, J. Régner, S. Poignant, O. Darnis, P. Maussion, Statistic-based spectral indicator for bearing fault detection in permanent-magnet synchronous machines using the stator current, *Mech. Syst. Signal Process.* 46 (2014) 424–441.
- [8] G. Xiang, Q. Wei, Bearing fault diagnosis for direct-drive wind turbines via current-demodulated signals, *IEEE Trans. Ind. Electron.* 60 (2013) 3419–3428.
- [9] A. Kusiak, A. Verma, Analyzing bearing faults in wind turbines: a data-mining approach, *Renew. Energy* 48 (2012) 110–116.
- [10] W. Caesarendra, B. Kosasih, A.K. Tieu, H. Zhu, C.A.S. Moodie, Q. Zhu, Acoustic emission-based condition monitoring methods: review and application for low speed slew bearing, *Mech. Syst. Signal Process.* <http://dx.doi.org/10.1016/j.ymssp.2015.10.020>.
- [11] J. Chen, J. Pan, Z. Li, Y. Zi, X. Chen, Generator bearing fault diagnosis for wind turbine via empirical wavelet transform using measured vibration signals, *Renew. Energy* 89 (2016) 80–92.
- [12] B. Dolenc, P. Bošković, Đ. Juričić, Distributed bearing fault diagnosis based on vibration analysis, *Mech. Syst. Signal Process.* 66–67 (2016) 521–532.
- [13] R. Zimroz, W. Bartelmus, T. Barszcz, J. Urbanek, Diagnostics of bearings in presence of strong operating conditions non-stationarity—a procedure of load-dependent features processing with application to wind turbine bearings, *Mech. Syst. Signal Process.* 46 (2014) 16–27.
- [14] T. Wang, M. Liang, J. Li, W. Cheng, C. Li, Bearing fault diagnosis under unknown variable speed via gear noise cancellation and rotational order sideband identification, *Mech. Syst. Signal Process.* 62–63 (2015) 30–53.
- [15] J.R. Stack, T.G. Habetler, R.G. Harley, Fault classification and fault signature production for rolling element bearings in electric machines, *IEEE Trans. Ind. Appl.* 40 (2004) 735–739.
- [16] K.R. Fyfe, E.D.S. Munck, Analysis of computed order tracking, *Mech. Syst. Signal Process.* 11 (1997) 187–205.
- [17] L.F. Villa, A. Reñones, J.R. Perán, L.J. de Miguel, Angular resampling for vibration analysis in wind turbines under non-linear speed fluctuation, *Mech. Syst. Signal Process.* 25 (2011) 2157–2168.
- [18] P. Borghesani, R. Ricci, S. Chatterton, P. Pennacchi, A new procedure for using envelope analysis for rolling element bearing diagnostics in variable operating conditions, *Mech. Syst. Signal Process.* 38 (2013) 23–35.

- [19] T. Wang, M. Liang, J. Li, W. Cheng, Rolling element bearing fault diagnosis via fault characteristic order (FCO) analysis, *Mech. Syst. Signal Process.* 45 (2014) 139–153.
- [20] J.M. Bossio, G.R. Bossio, C.H. De Angelo, A fault detection technique for variable-speed wind turbines using vibrations and electrical measurements, *Rev. Eletrônica De Potência* 19 (2014) 386–396.
- [21] L.R. Limongi, R. Bojoi, C. Pica, F. Profumo, A. Tenconi, Analysis and comparison of phase locked loop techniques for grid utility applications, *Power Conversion Conference – Nagoya (PCC '07)*, 2007, pp. 674–681.
- [22] P. Rodriguez, R. Teodorescu, I. Candela, A.V. Timbus, M. Liserre, F. Blaabjerg, New positive-sequence voltage detector for grid synchronization of power converters under faulty grid conditions, in: *Proceedings of the 37th IEEE Power Electronics Specialists Conference 2006 (PESC '06)*, 2006, pp. 1–7.
- [23] F.M. Serra, D.G. Forchetti, C.H. De Angelo, Comparison of positive sequence detectors for shunt active filter control, in: *Proceedings of the 9th IEEE/IAS International Conference on Industry Applications (INDUSCON 2010)*, 2010, pp. 1–6.
- [24] P. Rodríguez, A. Luna, R.S. Muñoz-Aguilar, I. Etxeberria-Otadui, R. Teodorescu, F. Blaabjerg, A stationary reference frame grid synchronization system for three-phase grid-connected power converters under adverse grid conditions, *IEEE Trans. Power Electron.* 27 (1) (2012) 99–112.